Yield Stress and Reversible Strain in Titanium Nickelide Alloys after Warm Abc Pressing

Aleksander Lotkov *, Victor Grishkov, Anatoly Baturin, Victor Timkin and Dorzhima Zhapova

Institute of Strength Physics and Materials Science of the Siberian Branch of the Russian Academy of Sciences, Tomsk, 634055, Russia; grish@ispms.tsc.ru (V.G.); abat@ispms.tsc.ru (A.B.); timk@ispms.tsc.ru (V.T.); dorzh@ispms.tsc.ru (D.Z.)

* Correspondence: lotkov@ispms.tsc.ru

Abstract: The results of the position analysis of the yield stress $\tau_{0.3}$ on the "stress–strain" (τ–γ) dependences, received at the torsion of specimens of $Ti_{49.8}Ni_{50.2}$ (at%) alloy are presented. The critical stress $\tau_{0.3}$ (IV), corresponding to the end of linear stage III and the beginning of the intensive development of plastic strain at stage IV, preceding the fracture of the specimens, were obtained as well. The structure of the specimens was transformed from coarse-grained to microcrystalline as a result of warm (723 K) abc pressing with a true deformation e of 8.4. The regularities of the development of reversible inelastic strain (superelasticity, SE, and shape memory effect, SME) and plastic strain γ_{pl} after isothermal (295 K) loading of specimens up to $\tau \le \tau_{0.3}(IV)$, unloading, and their subsequent heating up to 500 K are studied. From the joint analysis of the "τ–γ" dependences obtained at 295 K and "plastic strain–total strain" dependences the yield stress $\tau_{0.3}$ corresponding to the development of 0.3% of the plastic strain under loading of the specimens was determined. Critical stress $\tau_{0.3}(IV)$ was determined as equal to the stress corresponding to a deviation of 0.3% from the linear "τ–γ"dependence at stage III. It is shown that the yield stress $\tau_{0.3}$ for all specimens is localized at the beginning of stage III for all specimens. The ratio $\tau_{0.3}(IV)/\tau_{0.3}$ is from 2.3 to 3.8. The accumulation of plastic strain at stage III (after loading with τ from $\tau_{0.3}$ to $\tau_{0.3}(IV)$) is from 2.4% to 4.7% (depending on the true deformation of the specimens during warm abc pressing). Thus, stage III is the stage of deformation hardening of specimens under torsion. On the basis of the results of this and previous works it is shown that, in alloys with thermoelastic martensitic transformations and with thermomechanical memory, the ratio $\tau_{0.3}(IV)/\tau_{0.3}$ can vary in a wide range: in reinforced specimens $\tau_{0.3}$ can be close to $\tau_{0.3}(IV)$, and in more ductile specimens $\tau_{0.3}$ can be significantly less than $\tau_{0.3}(IV)$. However, in order to correctly determine the yield stress of $\tau_{0.3}$ and the corresponding strain $\gamma_t(0.3)$, it is necessary to carry out a joint analysis of "τ–γ" and "plastic strain–total strain" dependencies.

Keywords: martensitic transformations; superelasticity; shape memory; yield stress; plastic strain; abc pressing; torsion deformation

1. Introduction

TiNi-based materials, being bright representatives of smart materials, are widely used in engineering and medicine due to their high level of superelasticity (SE) and shape memory effect (SME), strength and plasticity, thermomechanical and thermal fatigue life, and corrosion resistance and biocompatibility. The excellent thermomechanical properties of TiNi are provided by thermoelastic martensite transformations from a cubic B2 phase to a rhombohedral R or a monoclinic B19′ phase. The shape of specimens with low internal stress remains unchanged under cooling and heating over the temperature ranges of martensitic transformations because of the formation of polivariant systems of self-accommodated martensite domains. SE and SME are conditioned by the deformation

influence. Shape memory is the ability for accumulation of reversible inelastic strain in isothermal loading–unloading cycles at $T_d < M_f$ (where T_d is the deformation temperature and M_f is the martensite finish temperature) and for its recovery in unloaded states of specimens at $T > A_f$ (where A_f is the austenite finish temperature). Superelasticity is the ability for accumulation of inelastic strain during the formation of stress-induced martensite (SIM) under isothermal loading at stresses higher than the martensite shear stress σ_M (or τ_M in torsion) and for its complete recovery under further unloading due to reverse SIM→B2 transition. The deformation temperature T_d for SE realization lies within the so-called superelastic window: $\Delta T = T_2 - T_1$ with $M_s < T_1 < T_d < T_2 < M_d$, where M_s is the martensite start temperature on cooling and M_d is the maximum SIM formation temperature under isothermal loading. Another important property of this type of alloy is the ability to produce high reactive stresses on the heating of specimens preliminary deformed in martensite ($T_d < M_s$) or SIM ($T_d > M_s$) states and constrained to prevent shape recovery.

In general, the degree of shape recovery η, being the ratio of reversible to total strains, and the reactive stress depend on development of plastic strain at the stages of preliminary loading and unloading or heating after predeformation of alloy specimens with thermoelastic martensitic transformations. Conventionally, the onset of plastic deformation in a material is judged from its macroscopic yield stress, i.e., from the stress $\sigma_{0.2}$ (in compression and tension) or $\tau_{0.3}$ (in torsion) at which the accumulated plastic strain reaches 0.2% and 0.3%, respectively. The higher the stress $\sigma_{0.2}$ compared to σ_M, the higher the SME, the SE, and the reactive stresses. The parameter $\Delta\sigma = \sigma_{0.2} - \sigma_M$ is analyzed in many studies [1–5], showing its significance on the way to better performance and wider applicability of TiNi alloys. The yield stress of materials can be increased by different methods: variation in their elemental composition (e.g., alloying), thermomechanical treatment [5–7], and severe plastic deformation with hardening via grain structure refinement to fine- and ultrafine-grained states [8–11]. However, correctly determining the yield stress of alloys like TiNi is problematic. The stress–strain diagram of materials with no thermoelastic martensite transformations includes a linear elastic stage followed by a plastic stage, and their yield stress criterion is the stress $\sigma_{0.2}$ or $\tau_{0.3}$ at which the dependence deviates from linearity by 0.2% (tension, compression) or by 0.3% (torsion) in the transition region between the elastic and plastic stages. For alloys with thermoelastic martensite transformations, such as TiNi, the stress–strain diagram is more complicated (Figure 1).
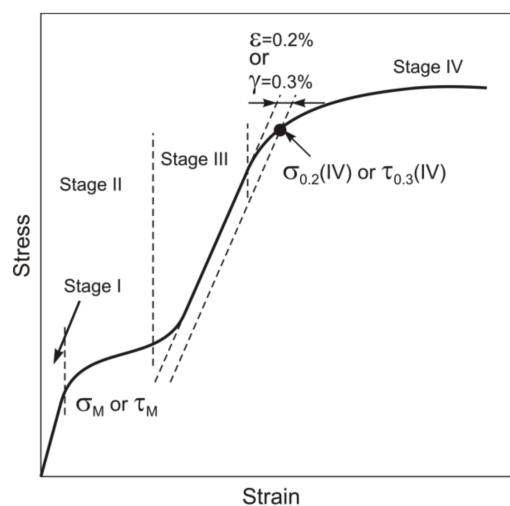

Figure 1. Schematic stress–strain diagram with stages I–IV at temperatures $T_d < M_d$ for alloys with martensitic transformations: σ_M, τ_M: martensitic shear stresses; $\sigma_{0.2}$(IV), $\tau_{0.3}$(IV): critical stresses are equal to yield stress $\sigma_{0.2}$, $\tau_{0.3}$ (according to [1,3,4,12–18]).

The diagram begins with short elastic stage I which passes to stage II at stresses $\sigma > \sigma_M$ ($\tau > \tau_M$). Stage II represents martensite detwinning and reorientation ($T_d < M_f$) or SIM generation ($T_d > A_f$) responsible for inelastic strain accumulation at comparatively small stresses. Then comes stage III

in which the response to increasing stresses is almost linear and the strain hardening coefficient $\theta = d\sigma/d\varepsilon$ $(d\tau/d\gamma)$ is higher than that in stage II. As $\sigma > \sigma_{0.2}(\text{IV})$ is reached, stage IV begins showing intense plastic flow with further fracture of specimens. In general, the total strain ε_t at any of stages II–IV comprises elastic martensite strains ε_{el}, reversible inelastic strains ε_{SE} and ε_{SME}, and plastic strains ε_{pl}: $\varepsilon_t = \varepsilon_{el} + \varepsilon_{SE} + \varepsilon_{SME} + \varepsilon_{pl}$. Thus, the dependences σ–ε and τ–γ allow us to correctly determine σ_M and τ_M, but determining $\sigma_{0.2}$ and $\tau_{0.3}$ from these dependences is impossible without analysis of the reversible strain $\varepsilon_{el} + \varepsilon_{SE} + \varepsilon_{SME}$ and plastic strain ε_{pl} with increasing the total strain ε_t.

Another concept is also available to judge the position of $\sigma_{0.2}$ on stress–strain diagrams [1,3,4,12–18]. The concept suggests that stage III corresponds to elastic martensite strains, and the yield stress to $\sigma_{0.2}(\text{IV})$ and $\tau_{0.3}$ (IV) (Figure 1). The idea of such an interpretation has apparently come from a study of Cu–Zn–Si alloys [19] in which almost complete strain recovery was found under unloading at total strains ε_t close to the end of stage III, suggesting that stage III is elastic for the martensite formed at stage II ($T_d > M_s$). The idea was then extended to Cu-, Ag-, and Au-based alloys with thermoelastic martensite transformations [20,21]. Similar judgments were made for TiNi-based alloys [1] from an analysis of their reversible inelastic and plastic behavior [22]: in loading–unloading cycles with heating to $T > A_f$ in unloaded states, TiNi alloys rich in C and Si completely recovered their shape at $\varepsilon_t \leq 8\%$ with maximum reactive stresses at $\varepsilon_t \approx 8\%$ late in stage III (note that ε_L was also introduced as a critical strain above which plastic deformation begins in a material [1]). In further studies [14–18], the stress $\sigma_{0.2}$ in TiNi-based alloys was assessed from the criterion of 0.2% deviation from linearity at stage III.

However, even early studies reported that after tension to ε_t at the end of stage II, unloading, and heating in unloaded states, the plastic strain was ~1% [23] in binary alloys with a Ni content of 50.1 at% (initial B19′ martensite). It was noted [24] that in stage III, the slopes ($d\sigma/d\varepsilon$ or $d\tau/d\gamma$) of "stress–strain" dependences under loading and unloading is essentially different for specimens of TiNi-based alloys. This contradicts the supposition that only elastic deformation of reoriented martensite occurs at stage III. Additionally, a high dislocation density was found by transmission electron microscopy in TiNi deformed at stage III [24]. These results were confirmed by further studies [25–34]. The finish of reorientation and detwinning of martensite domains (in specimens with initial martensite structure) and formation of SIM (in specimens with initial B2 structure), the appearance of high dislocation density and formation of compound twins, such as $\{20?1\}_{B19'}$, $\{110\}_{B19'}$, and $\{1?13\}_{B19'}$, were observed after deformation at stage III of different TiNi-based alloys with polycrystalline [25–31] and monocrystal [32–34] structures. Consequently, the development of both inelastic strains and plastic strain may develop at stage III.

In several studies [25,26,29,30,32–34], the ε_t dependences of ε_{el}, ε_{SE}, ε_{SME}, and ε_{pl} were analyzed in isothermal cycles of loading and unloading with further heating to complete shape recovery via reverse martensite transformation to B2. The plastic strain at ε_t close to the end of stage III was shown to measure 1–5%, but the yield stress $\sigma_{0.2}$ from the σ–ε and ε_{pl}–ε_t dependences was not determined. One of the recent studies [35] provides data on the γ_t dependences of γ_{SE}, γ_{SME}, and γ_{pl} in coarse-grained and microcrystalline $Ti_{49.2}Ni_{50.8}$ (at%) under torsion in isothermal τ–γ cycles (295 K) with heating in unloaded states. The τ–γ and γ_{pl}–γ_t dependences of $Ti_{49.2}Ni_{50.8}$ (with an average grain size of 43 µm to 1.5 µm after warm caliber rolling at 723 K) show that $\tau_{0.3}$ lies near the beginning of stage III and that after deformation with γ_t corresponding to $\tau_{0.3}(\text{IV})$, the plastic strain is 1% irrespective of the average grain size in the material. The difference $\Delta\tau = \tau_{0.3}(\text{IV}) - \tau_{0.3}$ is considerable and increases from 160 MPa in the coarse-grained material to 460 MPa in the microcrystalline one.

Here we analyze the yield stress $\tau_{0.3}$, plastic strain, and reversible inelastic strain under torsion in $Ti_{49.8}Ni_{50.2}$ (at%) with an average grain size of 40 µm to ~1.5 µm after warm abc pressing at 723 K.

2. Materials and Methods

The almost equiatomic alloy $Ti_{49.8}Ni_{50.2}$ at%, containing Ti_4Ni_2 (N,O) in an amount of ~6 vol%, was supplied as hot-swaged bars of diameter 20 mm (MATEK-SMA, Moscow, Russia). After high-temperature abc forming at 1023 K, its specimens were shaped as cubes with an edge of ~20 mm.

The specimens were exposed to warm multicycle abc pressing in a die at 723 K with upsetting in three orthogonal directions during each cycle. The strain rate was $\dot{\varepsilon}$ = 0.16–0.18 s^{-1}, and the total true plastic strain per cycle was e = 0.2–0.3, being the sum of natural logarithm of ratios of specimen heights before and after upsetting. Before each upsetting event, the die with a specimen was heated in a furnace at 723 K. The specimen temperature during abc pressing varied by no more than 10 deg. In the initial state after hot forming at 1023 K, the specimens had a coarse-grained structure with an average grain size <d> = 40 μm. As the strain e was increased, the grain size <d> decreased, measuring 1.5 μm after warm abc pressing with e = 8.4 at 723 K. A detailed discussion of the effect of pressing at 723 K on the grain-subgrain structure of the alloy can be found elsewhere [36]. After warm abc pressing at 723 K, the true strain in the specimens was 0.3, 0.6, 1.8, 4.2, 6.4, and 8.4.

The inelastic and plastic strains in the material under torsion was studied on an inverted torsion pendulum with an operating temperature of 573–120 K. The test specimens were bars of diameter ~1 mm with a gage length of ~10 mm. The experimental method used to determine the reversible inelastic strains γ_{SE}, γ_{SME} and plastic strain γ_{pl} is shown in Figure 2. The total strain is $\gamma_t = \gamma_{SID} + \gamma_{pl} = \gamma_{el} + \gamma_{SE} + \gamma_{SME} + \gamma_{pl}$. The "τ–γ" dependencies for each strain γ_t were obtained in isothermal (295 K) "loading-unloading" cycles. The value of γ_{SE} (the superelasticity effect) was assumed to be equal to the recovery of the strain under isothermal unloading (including a small Hook strain of ~1.5% [37]): $\gamma_{SE} = \gamma_t - \gamma_r$. After unloading, the martensite phase was partially present providing the presence of residual strain γ_r in the unloaded specimens at 295 K. The martensitic phase transforms into the B2 phase with the subsequent heating of the unloaded specimens. This martensite transformation provides the recovery of inelastic strain during heating: $\gamma_{SME} = \gamma_r - \gamma_{pl}$. The plastic strain γ_{pl} is equal to the residual strain after completion of the shape recovery. The value of γ_{pl} for all specimens was determined at 500K (~150 degrees above A_f in the initial specimens). The strains γ_t, γ_r, and γ_{pl} strains are equal to $arctgS_t$, $arctgS_r$, and $arctgS_{pl}$, where $S_t = (d\phi_t)/2l$, $S_r = (d\phi_r)/2l$, $S_{pl} = (d\phi_{pl})/2l$; ϕ_t, ϕ_r, and ϕ_{pl} are the torsional angles of the specimens in radians under isothermal loading with γ_t, after complete unloading and at 500 K, respectively; d and l are the dimensions of the cross-section and the length of the specimen gage section. In each next cycle γ_t was increased. The final value of γ_t is equal to γ_t(IV), corresponding to $\tau_{0.3}$(IV) of each specimen with the true strain e after warm abc pressing (Figure 1). The degree of the shape recovery of the specimens was determined to be η = γ_{SID} / γ_t.
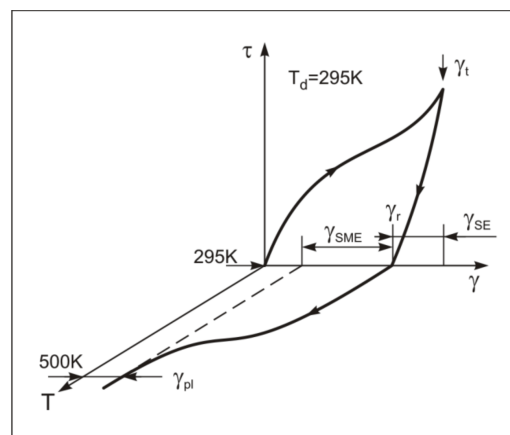

Figure 2. The accumulation and recovery of strain in isothermal (T_d = 295 K) cycle "τ-γ" and during the subsequent heating of unloaded specimens (scheme).

The sequence and temperatures of martensite transformations in the alloy after warm abc pressing at 723 K were considered previously [36]. Of importance here is the following aspect: In Ti$_{49.8}$Ni$_{50.2}$ (at%) preliminarily quenched from 1073 K, only B2↔B19′ transitions occur on cooling and heating. The martensite start and finish temperatures in the quenched alloy are M_s = 317 K and M_f = 219 K (B2→B19′ transition), and the austenite start and finish temperatures are A_s = 343 K and A_f = 354 K

(reverse B19′→B2 transition). The initial alloy preformed at high temperature undergoes B2→R→B19′ transitions on cooling. The rhombohedral R phase is formed at T_R = 327 K, and the temperatures of R→B19′ and reverse B19′→B2 transitions lie in the range from M_s = 316 K to M_f = 281 K and from A_s = 338 K to A_f = 355 K, respectively. Thus, the temperatures of B2→B19′, R→B19′, and B19′→B2 in the alloy after quenching and after high-temperature forming are almost the same.

After warm abc pressing with e = 0.3–8.4 at 723 K, the sequence of martensite transformation in the alloy on cooling and heating remains unchanged: B2→R→B19′ and B19′→B2, respectively. The temperatures T_R, $A_{s,}$, and A_f remain constant, and M_s and M_f decrease linearly to 311 K and 276 K (by ~5 and ~10 deg, respectively) with an increase in e to 8.4. Thus, both the initial and the abc-pressed specimens have a two-phase R + B19′ structure at 295 K.

3. Experimental Results

Figure 3 shows the engineering stress–strain diagrams of the initial and abc-pressed TiNi specimens under isothermal loading at 295 K. It is shown that the dependences comprise stages I–IV typical for alloys with thermoelastic martensite transformations (Figure 1).
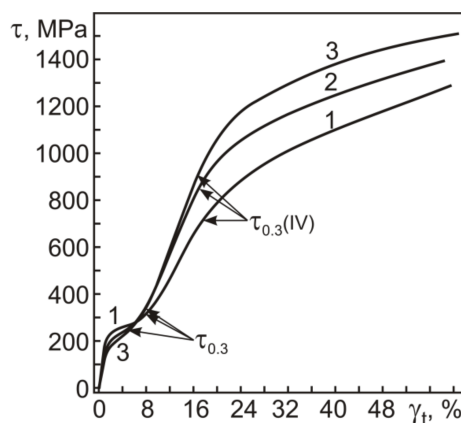

Figure 3. Engineering stress–strain diagrams in torsion at 295 K for Ti$_{49.8}$Ni$_{50.2}$ before (1) and after warm abc pressing at 723 K with true strains e = 1.8 (2) and e = 8.4 (3).

Since both the initial and abc-pressed specimens at 295 K have a two-phase R + B19′ structure ($T_d > M_f$), the deformation stage II in both involves the formation of SIM due to their R→B19′ transition under loading and the reorientation and detwinning of the B19′ martensite present before loading. The martensite shear stress τ_M as a function of the initial true strain e is shown in Figure 4.
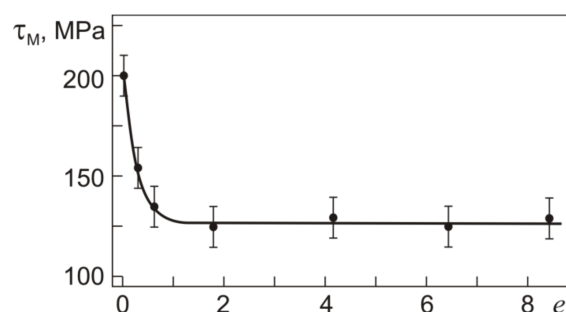

Figure 4. Martensite shear stress τ_M vs. true strain e in T$_{49.8}$Ni$_{50.2}$ in torsion at 295 K.

Figure 4 shows that the martensite shear stress τ_M, or the pseudo-yield stress, decreases noticeably after pressing with $e \leq 0.6$ and remains constant with further increasing e to 8.4. As can be seen from Figure 3, the pseudo-yield stage gradually passes to stage III at which the strain increases linearly with the applied stress. At this stage, the strain hardening coefficient θ = dτ/dγ increases with e

specified in warm abc pressing (Figure 3). The stress $\tau_{0.3}$(IV), corresponding to a deviation of 0.3% from the previous linear stage III, causes the material to enter stage IV, which culminates in its fracture. In Figure 3, the stress $\tau_{0.3}$(IV) in the initial specimen and specimens pressed with e = 1.8 and e = 8.4 is 710, 870, and 915 MPa, respectively.

To correctly determine the yield stress $\tau_{0.3}$, which corresponds to an accumulated plastic strain of 0.3%, we should analyze the dependence of the plastic strain γ_{pl} on the total strain γ_t in torsion. All components of reversible inelastic strains $\gamma_{SID} = \gamma_{SE} + \gamma_{SME}$ and γ_{pl} as a function of γ_t obtained in the study are for isothermal loading–unloading cycles at 295 K with heating in unloaded states to 500 K (as described in the Materials and Methods). As can be seen from Figure 5, the γ_t dependences of γ_{pl} for all specimens are qualitatively similar. Increasing the total strain γ_t to ~16% slightly increases the plastic strain γ_{pl}, and as γ_t goes above 16%, γ_{pl} begins to grow. The data in Figure 3 show that γ_t = 16% is close to γ_t(IV), corresponding to $\tau_{0.3}$(IV). Thus, the critical stress $\tau_{0.3}$(IV) in the initial and abc-pressed specimens characterizes the onset of intense plastic flow at stage IV rather than the onset of yielding, i.e., the yield stress $\tau_{0.3}$.
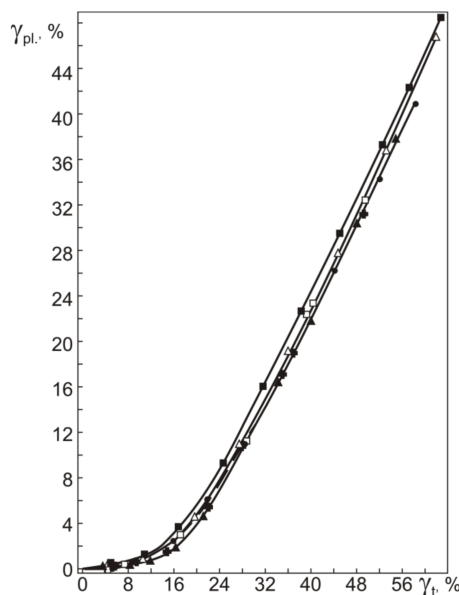

Figure 5. Plastic strain γ_{pl} vs. total strain γ_t in torsion at 295 K for Ti$_{49.8}$Ni$_{50.2}$ before (●) and after abc pressing with e equal to 0.6 (■), 1.8 (△), 4.2 (□), 6.4 (✦), and 8.4 (▲).
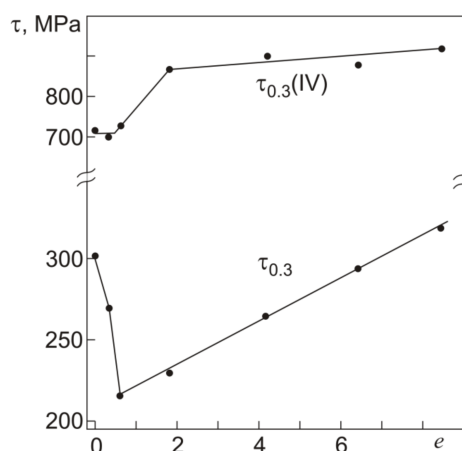

Figure 6. Yield stress $\tau_{0.3}$ and critical stress $\tau_{0.3}$(IV) in torsion at 295 K for Ti$_{49.8}$Ni$_{50.2}$ after abc pressing with different true strains e.

The γ_t dependences of γ_{pl} allow us to rather easily determine the yield stress $\tau_{0.3}$ on τ–γ diagrams like those in Figure 3. From the γ_t dependences of γ_{pl} we can estimate the total strain $\gamma_t(0.3)$ at which $\gamma_{pl} = 0.3\%$, and the values of $\gamma_t(0.3)$ will give the position of the yield stress $\tau_{0.3}$ on the τ–γ diagrams. Figures 6 and 7 show the yield stress $\tau_{0.3}$ and strain $\gamma_t(0.3)$, and the stress $\tau_{0.3}(IV)$ and strain $\gamma_t(IV)$ in the initial and abc-pressed specimens.

From Figure 6 it is seen that $\tau_{0.3}(IV)$ remains almost unchanged after abc pressing with $e \leq 0.6$ and increases as e is increased to 1.8. In the specimens pressed with $e = 1.8$–8.4, the increment in $\tau_{0.3}(IV)$ is ~200 MPa. The diagrams in Figure 7 show that the strain $\gamma_t(IV)$ corresponding to the end of stage III and the transition to stage IV decreases by 0.4% after abc pressing with $e = 4.2$ compared to $\gamma_t(IV)$ in the initial specimens. After pressing with $e = 6.4$ and $e = 8.4$, the decrease in $\gamma_t(IV)$ is ~1%. By and large, all $\tau_{0.3}(IV)$ correspond to the range of $\gamma_t(IV)$ from 17% to 18.5%. The yield stress $\tau_{0.3}$ in the specimens pressed with $e = \leq 0.6$ at 723 K decreases to 220 MPa against its value $\tau_{0.3} = 300$ MPa in the initial specimens. Consequently, the work softening is observed in the specimens after warm abc pressing with $e \leq 0.6$. After abc pressing with $e = 0.6$–8.4, the yield stress $\tau_{0.3}$ increases linearly almost to its initial value. The secondary hardening of specimens is the result of warm pressing with $e > 0.6$. Thus, the yield stress $\tau_{0.3}$ in the initial (coarse-grained) and abc-pressed (microcrystalline structure) specimens differs little, measuring 300 and 320 MPa, respectively. As can be seen from Figure 7, the e dependence of $\gamma_t(0.3)$, corresponding to $\tau_{0.3}$, differs from that of $\gamma_t(IV)$.
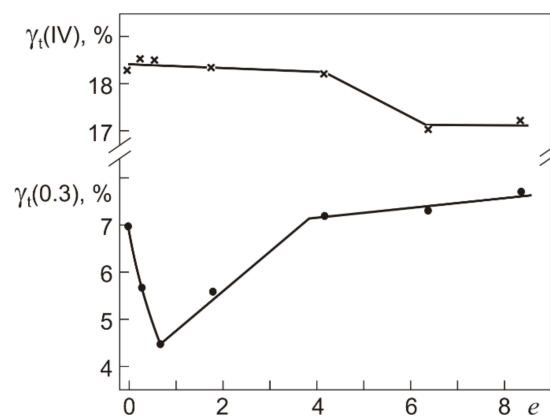

Figure 7. Total strains $\gamma_t(0.3)$ and $\gamma_t(IV)$ at which $\tau_{0.3}$ and $\tau_{0.3}(IV)$ are reached in $Ti_{49.8}Ni_{50.2}$ after warm abc pressing with different true strains e.

The initial alloy reaches $\tau_{0.3}$ at $\gamma_t(0.3) = 7\%$. After abc pressing with $e = 0.6$, the yield stress $\tau_{0.3}$ shows its minimum (Figure 6) at $\gamma_t(0.3) = 4.5\%$ (Figure 7), and as e is increased from 0.6 to 4.2, the value of $\gamma_t(0.3)$ grows to that of the initial alloy. After abc pressing with $e = 4.2$–8.4, the increment in $\gamma_t(0.3)$ slows down to ~0.5%. As a whole, the variation in $\gamma_t(0.3)$ is ~3%, which is twice as large as the variation in $\gamma_t(IV)$ after pressing with e up to 8.4. The extent of stage III in the initial alloy is 11.5%, reaches its maximum of ~14% after pressing with $e = 0.6$, and decreases to 9.5% after pressing with $e = 8.4$.

The plastic strain $\gamma_{pl}(IV)$ after loading to $\tau_{0.3}(IV)$ can be estimated from a joint analysis of the τ–γ and γ_{pl}–γ_t dependences in Figures 3 and 5. Figure 8 shows the plastic strain $\gamma_{pl}(IV)$ as a function of e specified in warm abc pressing.
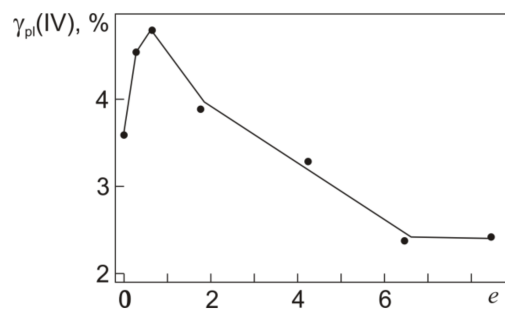
Figure 8. Plastic strain $\gamma_{pl}(IV)$ corresponding to $\tau_{0.3}(IV)$ early in stage IV in torsion at 295 K for Ti$_{49.8}$Ni$_{50.2}$ after abc pressing with different true strains e.

Figure 8 shows that, against the decrease in $\tau_{0.3}$ and almost invariant $\tau_{0.3}(IV)$ in the specimens pressed with $e \leq 0.6$, their plastic strain $\gamma_{pl}(IV)$ increases from 3.6% to its maximum 4.7% at $e = 0.6$. The specimens pressed with $e > 0.6$, in which the yield stress $\tau_{0.3}$ grows, reveal a monotonic decrease in $\gamma_{pl}(IV)$. However, even in the specimens with $e = 6.4$ and 8.4, the plastic strain accumulated in torsion at $\gamma_t = \gamma_t(IV)$ corresponding to $\tau_{0.3}(IV)$ remains high (~2.4%). Thus, the actual yield stress in Ti$_{49.8}$Ni$_{50.2}$ is close to the onset of stage III on its τ–γ dependences (Figure 3). Stage III is a strain hardening stage at which γ_{pl} increases from 0.3% to 2.4–4.7%.
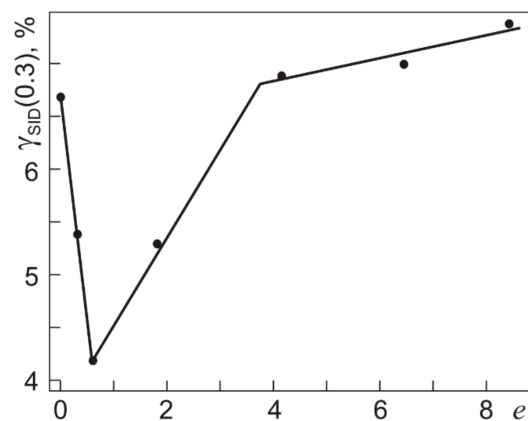

Figure 9. Total reversible inelastic strain $\gamma_{SID}(\tau_{0.3})$ recovered by Ti$_{49.8}$Ni$_{50.2}$ after torsion with $\tau = \tau_{0.3}$ (295 K) and heating (500 K) at different true strains e specified in warm abc pressing. Residual plastic strains $\gamma_{pl} = 0.3$%.

Figures 9 and 10 show the total reversible inelastic strains $\gamma_{SID}(0.3)$ and $\gamma_{SID}(IV)$ recovered after isothermal loading to $\gamma_t(0.3)$ and $\gamma_t(IV)$, which correspond to $\tau_{0.3}$ and $\tau_{0.3}(IV)$, unloading, and heating in unloaded states as a function of e in abc pressing ($\gamma_{SID} = \gamma_{SE} + \gamma_{SME} = \gamma_t - \gamma_{pl}$). As can be seen, the dependences are qualitatively similar. In the specimens pressed with $e \leq 0.6$, the strains $\gamma_{SID}(0.3)$ and $\gamma_{SID}(IV)$ are smaller than those in the initial specimens. The strains $\gamma_{SID}(0.3)$ and $\gamma_{SID}(IV)$ increase after abc pressing with e from 0.6 to 4.2. After pressing with e from 4.2 to 8.4, the strain $\gamma_{SID}(0.3)$ increases somewhat while $\gamma_{SID}(IV)$ decreases somewhat. The dependence of $\gamma_{SID}(0.3)$ is close to that of $\gamma_t(0.3)$ because the accumulated plastic strain is low (0.3%) and is the same for all specimens. The behavior of $\gamma_{SID}(IV)$ is governed by variations of both $\gamma_t(IV)$ (Figure 7) and $\gamma_{pl}(IV)$ accumulated under loading to $\tau_{0.3}(IV)$ (Figure 8).
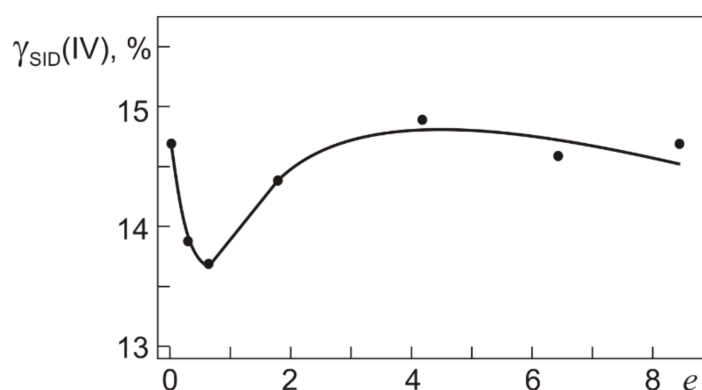
Figure 10. Total reversible inelastic strain $\gamma_{SID}(IV)$ recovered by $Ti_{49.8}Ni_{50.2}$ after torsion with $\tau = \tau_{0.3}(IV)$ (295 K) and heating (500 K) at different true strains e specified in warm abc pressing.

The minimum value of $\gamma_{SID}(IV)$ after abc pressing with $e = 0.6$ is due to the maximum value of $\gamma_{pl}(IV)$ and to the constancy of $\gamma_t(IV)$. After pressing with $0.6 < e < 4.2$, the plastic strain $\gamma_{pl}(IV)$ decreases more greatly than $\gamma_t(IV)$, and this allows $\gamma_{SID}(IV)$ to reach its maximum almost equal to $\gamma_{SID}(IV)$ in the initial specimens. When $\gamma_{pl}(IV)$ and $\gamma_t(IV)$ are decreased simultaneously, the specimens pressed with $e = 6.4$ and 8.4 show a slight decrease in $\gamma_{SID}(IV)$.

An important characteristic of shape memory alloys is the degree of shape recovery $\eta = (\gamma_t - \gamma_{pl})/\gamma_t = \gamma_{SID}/\gamma_t$, being the ratio between reversible inelastic strains produced under loading to γ_t and recovered under unloading (SE) and further heating (SME). Figure 11 shows the degree of shape recovery $\eta_{0.3}$ and $\eta_{0.3}(IV)$ after loading to $\tau_{0.3}$ and $\tau_{0.3}(IV)$, respectively, as a function of e in warm abc pressing. After abc pressing with $e \leq 0.6$, $\eta_{0.3}$ decreases from 96% to 93%, and after abc pressing with e from 1.8 to 8.4, its value is $\eta_{0.3} = 96\%$ as in the initial specimens.

The e dependences of $\eta_{0.3}$ and $\eta_{0.3}(IV)$ are qualitatively similar. However, $\eta_{0.3}(IV)$ is 10–20% lower than $\eta_{0.3}$ both in the initial and in the abc-pressed specimens. This is because plastic strain develops under loading at stage III (Figure 8). In the initial specimens, $\eta_{0.3}(IV) = 80\%$. In the specimens pressed with $e \leq 0.6$, it decreases to 74% and, in those pressed with e from 1.8 to 8.4, it increases to 85%. Thus, in terms of complete shape recovery, the range of total strains $\gamma_t \leq \gamma_t(0.3)$ at applied stresses $\tau < \tau_{0.3}$ is more preferable.
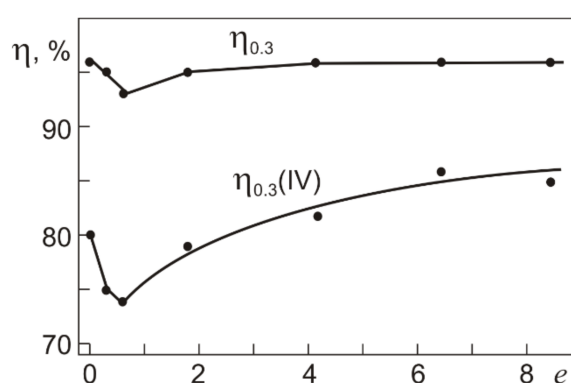

Figure 11. The degree of shape recovery $\eta_{0.3}$ at $\tau_{0.3}$ and $\eta_{0.3}(IV)$ at $\tau_{0.3}(IV)$ in $Ti_{49.8}Ni_{50.2}$ in isothermal loading–unloading cycles (295 K) with heating in unloaded states (500 K) as a function of the true strain e in warm abc pressing.

Another important result concerns the total strain $\gamma_{SID} = \gamma_{SE} + \gamma_{SME}$. From comparison of Figures 9 and 10 it follows that $\gamma_{SID}(IV)$ is two times higher than $\gamma_{SID}(0.3)$. The inelastic strains $\gamma_{SE}(0.3)$, $\gamma_{SME}(0.3)$ and $\gamma_{SE}(IV)$, γ_{SME} (IV) for loading to $\tau_{0.3}$ and $\tau_{0.3}(IV)$ are plotted in Figure 12.
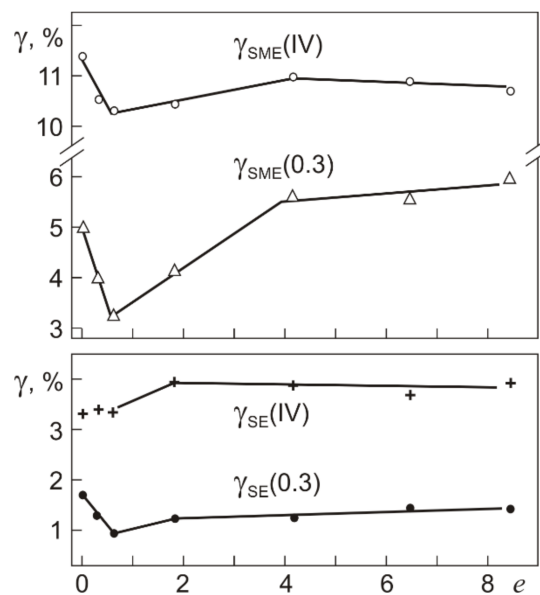
Figure 12. Reversible inelastic strains $\gamma_{SE}(0.3)$ and $\gamma_{SME}(0.3)$ at $\tau_{0.3}$, and $\gamma_{SE}(IV)$ and $\gamma_{SME}(IV)$ at $\tau_{0.3}(IV)$ in $Ti_{49.8}Ni_{50.2}$ in isothermal loading–loading cycles (295 K) with heating in unloaded states (500 K) as a function of the true strain e in warm abc pressing.

As can be seen from Figure 12, $\gamma_{SME} > \gamma_{SE}$ in all specimens irrespective of their grain structure and total strains $\gamma_t(0.3)$, $\gamma_t(IV)$. The strain $\gamma_{SME}(0.3)$ is close to $\gamma_{SID}(0.3)$ because $\gamma_{SE}(0.3)$ is small and is almost equal to the recovery of elastic martensite strain under unloading: 1–1.5% [37]. Increasing the total strain under loading to $\tau_{0.3}(IV)$ increases $\gamma_{SE}(IV)$ to 3–4% in the initial specimens and specimens after the pressing. The strain $\gamma_{SME}(IV)$ in these specimens weakly depends on e, and its value $\gamma_{SME}(IV)$ = 10–11% is 2–3 times higher than $\gamma_{SME}(0.3)$. Thus, coarse-grained and microcrystalline $Ti_{49.8}Ni_{50.2}$ structures plastically deformed by torsion are promising SME materials capable of providing high reversible inelastic strains after loading with $\tau_{0.3}(IV)$.

4. Discussion

Data on yield stress in alloys with martensitic transformations, including TiNi, are necessary for assessing their operability and reliability as structures with SE- and SME-based functional properties. In our analysis, we follow two approaches to yield stress estimations in near-equiatomic $Ti_{49.8}Ni_{50.2}$ (at%) transformed from coarse-grained to microcrystalline states by warm abc pressing at 723 K. The first approach implies an analysis of the τ–γ dependence (Figure 1) with linear stage III taken as elastic martensite deformation and yield stress as stresses at which stage III ends and passes to stage IV. The second approach implies a joint analysis of the τ–γ dependence and γ_{pl}–γ_t dependence in loading–unloading cycles at increasing γ_t with the yield stress taken as stress $\tau_{0.3}$, at which the accumulated plastic strain reaches 0.3%.

Our study shows that in $Ti_{49.8}Ni_{50.2}$ alloy, whether coarse-grained or microcrystalline after warm pressing, the accumulated plastic strain at stage III under torsion with $\tau = \tau_{0.3}(IV)$ ranges from 2.4% to 4.7%, i.e., it is much higher than 0.3%. Assuming that $\tau_{0.3}(IV)$ is the yield stress, the degree of shape recovery after loading to $\tau_{0.3}(IV)$, unloading, and further heating, would measure $\eta_{0.3}(IV)$ = (97.3 ± 0.1)% in all specimens irrespective of their structure. However, its actual value after loading to $\tau = \tau_{0.3}(IV)$ varies from 74% to 85% depending on e. The stress $\tau_{0.3}(IV)$ is 700–920 MPa, and the yield stress $\tau_{0.3}$ compared to $\tau_{0.3}(IV)$ is 2–3 times smaller, measuring 230–320 MPa and approximating the onset of stage III. After such cycles with loading to $\tau = \tau_{0.3}$, the degree of shape recovery remains high: 93–96%.

These results are qualitatively similar to the results of our previous study [35] in which we analyzed the yield stress $\tau_{0.3}$ and critical stress $\tau_{0.3}$(IV) under torsion in $Ti_{49.2}Ni_{50.8}$ (at%) alloy transformed from coarse- to fine-grained states by warm caliber rolling at 723 K. For the alloy, which had a two-phase B2+R structure before torsion at T_d = 295 K, the ratio $\tau_{0.3}$(IV)/$\tau_{0.3}$ was 1.45 ± 0.20 depending on the true strain in rolling. The stress $\tau_{0.3}$ was also close to the onset of stage III, but the degree of shape recovery after loading, unloading, and heating to 500 K in $Ti_{49.8}Ni_{50.2}$ alloy was higher than its value in $Ti_{49.8}Ni_{50.2}$: 97% and 93% after loading to $\tau_{0.3}$ and $\tau_{0.3}$(IV), respectively. The plastic strain accumulated at stage III with $\tau = \tau_{0.3}$(IV) was 1%.

Thus, our research in abc-pressed $Ti_{49.8}Ni_{50.2}$ (at%) and caliber-rolled $Ti_{49.2}Ni_{50.8}$ (at%) [35] demonstrates that jointly analyzing the dependences τ–γ and γ_{pl}–γ_t in loading, unloading, and heating cycles allows one to estimate the yield stress $\tau_{0.3}$, critical stress $\tau_{0.3}$(IV), plastic strain accumulated at stage III, and total inelastic strain γ_{SID} and its components γ_{SE} and γ_{SME} depending on the total torsional strain γ_t.

It is seen from Figures 10 and 12 that, in $Ti_{49.8}Ni_{50.2}$ alloy after warm abc pressing, the inelastic strains γ_{SID}, γ_{SE}, and γ_{SME} increase 2–2.5 times after loading with total strains from γ_t(0.3) to γ_t(IV) at stage III. The dependences of γ_{SID}, γ_{SE}, and γ_{SME} are similar to those obtained for the same material in torsion with $\gamma_t > \gamma_t$(IV) at T_d = 295 K [38]: after deformation with $\gamma_t > \gamma_t$(IV), the strains γ_{SID}, γ_{SE}, and γ_{SME} continue to grow, reach their maximum values, and then decrease. However, the increments in γ_{SID}, γ_{SE}, and γ_{SME} are much lower than that after loading with γ_t from γ_t(0.3) to γ_t(IV). The maximum value of γ_{SID} equal to 16–18% is reached in the range γ_t = 27–48% with the plastic strain measuring γ_{pl} = 10–30%. The increment in γ_{SME} is no greater than 1–2%: γ_{SME} increases to 11–13%. The increase in γ_{SID} to its maximum is governed mostly by γ_{SE}, which increases from 4% after deformation at $\gamma_t = \gamma_t$(IV) to 6–7% at γ_t = 27–48%. Thus, ~85% of the reversible inelastic strain in $Ti_{49.8}Ni_{50.2}$ alloy is attained after loading with γ_t corresponding to stage III on the τ–γ dependence.

In summary, it should be noted that, in $Ti_{49.8}Ni_{50.2}$ alloy after warm abc pressing, the ratio $\tau_{0.3}$(IV)/$\tau_{0.3}$ is 2.4–3.8 and, in $Ti_{49.2}Ni_{50.8}$ alloy after warm rolling, it is 1.45 ± 0.2 [35]. At the same time, research data are available on two TiNi-based alloys in which the yield stress and the critical stress at the end of stage III are very close [14,16]. After compression at 293 K and unloading, complete shape recovery was observed in single-crystal $Ti_{48.5}Ni_{51.5}$ (at%) alloy aged at 823 K for 1.5 h [14]. Polycrystalline $Ti_{50.2}Ni_{49.8}$ (at%) alloy hardened by a single pass of equal channel angular pressing (channel angle 90°) at room temperature revealed its complete shape recovery after isothermal (293 K) cycles of compression with strains close to the end of stage III and unloading with further heating [16].

Thus, the ratio $\tau_{0.3}$(IV)/$\tau_{0.3}$ or $\sigma_{0.2}$(IV)/$\sigma_{0.2}$ can vary over a wide range depending on the composition of an alloy and its preliminary thermomechanical treatment. However, the yield stress in alloys with martensitic transformations, including TiNi, can be correctly determined only from a joint analysis of stress–strain dependences (τ–γ or σ–ε) and dependences of accumulated plastic strains on total strains (τ_{pl}–γ_t or σ_{pl}–σ_t). The similarity of the methods for determining the actual yield stress under torsion, compression, and tension of TiNi-based alloy specimens is provided by the following results. The deformation behavior of these alloys is qualitatively similar for these deformation modes. The same four deformation stages (I–IV) are observed on the "σ–ε" dependences obtained under tension and compression of TiNi-based alloy specimens, as well as on their "τ–γ" dependences obtained under torsion. The development of plastic ε_{pl} strain and reversible inelastic strains (SE, SME, total inelastic strain) were studied and depend on the total ε_t tension strain in isothermal "loading–unloading" cycles with subsequent heating of the unloaded specimens of binary alloys with 50.5 at% Ni (polycrystalline structure [29]) and 50.6 at% Ni (single-crystal with [100] orientation [31]). In [29,31] it was noted that the onset of ε_{pl} development corresponded to the transition from stage II (pseudo-yield "plateau") to stage III, but $\sigma_{0.2}$ was not determined in these studies. By the end of stage III ε_{pl} reached 2.5% in polycrystalline specimens [29] and ~5% in single-crystal specimens [31]. At the same time, the maximum total reversible inelastic strain was attained after loading at stresses corresponding to the end of stage III. Similar studies of the plastic strain ε_{pl} and reversible inelastic strains were carried out in [32]

under compression of single-crystal (orientation [001]) specimens of the TiNi(Mo,Fe) alloy with the initial B2 structure. The results [32] showed that 0.2% of the plastic strain appears after loading with $\sigma_{0.2}$ = 580 MPa (the beginning of stage III on the "σ–ε" dependence). After compression with $\sigma \approx$ 900 MPa (the end of stage III and the transition to stage IV) the plastic strain increased up to 2%. Consequently, $\sigma_{0.2}$(IV) / $\sigma_{0.2} \geq$ 1.6 in these specimens. In general, the results [29,31,32] for TiNi-based alloy specimens under compression and tension are qualitatively similar to those obtained for $Ti_{49.8}Ni_{50.2}$ (at%) alloy specimens after warm abc pressing in our study and for $Ti_{49.2}Ni_{50.8}$ (at%) alloy specimens after warm rolling under torsion [35].

In conclusion, the following should be noted: Non-monotonous changes of yield stress $\tau_{0.3}$, intensity of plastic strain accumulation, and corresponding changes of reversible inelastic strains under torsion are determined by the work softening and further strengthening of specimens during warm abc pressing. The physical causes for these processes are not discussed in our paper because no experimental data are presently available for such a discussion. At present, research is conducted on the fine crystalline and dislocation structures in the material after warm abc pressing and after torsion. The results of this research will be presented in our future publications.

5. Conclusions

Our study shows that in $Ti_{49.8}Ni_{50.2}$ (at%) transformed from coarse-grained to microcrystalline states by warm abc pressing at 723 K the yield stress $\tau_{0.3}$ on its τ–γ diagram occurs early in stage III featuring a linear increase in torsional strains under applied stress. The end of stage III and the onset of stage IV, with its intense plastic flow and eventual fracture, fall on the critical stress $\tau_{0.3}$(IV) corresponding to a deviation of 0.3% from the previous linear τ–γ stage. The ratio $\tau_{0.3}$(IV)/$\tau_{0.3}$ in the alloy is 2.3–3.8.

At total strains in the range from $\tau_{0.3}$ to $\tau_{0.3}$(IV), the accumulated plastic strain in the abc pressed alloy is 2.4–4.7%. Hence, stage III represents strain hardening.

After isothermal torsional loading to $\tau_{0.3}$ and unloading at 295 K with further heating to 500 K, the degree of shape recovery in the TiNi alloy is 93–96% both in its initial state and in its states after abc pressing with different true strains *e*. The total inelastic strain γ_{SID} in such TiNi specimens is no greater than ~7% and is mostly due to the component γ_{SME} while the component γ_{SE} approximates the elastic strain and measures ~1.5%. As the applied stress is increased from $\tau_{0.3}$ to $\tau_{0.3}$(IV), the degree of shape recovery in the TiNi specimens after loading, unloading, and heating decreases to 74–85% while the total reversible inelastic strain grows to 14–15% of which 10–11% is recovered via heating (shape memory effect) and ~4% via unloading (superelasticity). Thus, at $\tau_{0.3}$(IV), both components γ_{SME} and γ_{SE} increase, but γ_{SE} remains much lower than γ_{SME}. Such plastically deformed specimens with high inelastic strain recovery may be useful for manufacture of functional elements with shape memory.

Reasoning from this study and studies reported elsewhere [14,16,35], we can conclude that the ratio $\tau_{0.3}$(IV)/$\tau_{0.3}$ in alloys with martensite transformations is widely variable: in hardened specimens, the yield stress $\tau_{0.3}$ can approximate $\tau_{0.3}$(IV), and its value in more plastic specimens can be much lower than $\tau_{0.3}$(IV). By and large, the yield stress $\tau_{0.3}$ and the total strain γ_t(0.3) for its reach should be assessed by jointly analyzing of "stress–strain" and "plastic strain–total strain" dependences.

Author Contributions: Conceptualization: A.L., V.G.; formal analyses: A.L., V.G., A.B.; Investigations, V.G., D.Z., V.T.; methodology: A.L., V.G.; project administration: A.L., V.G.; supervision: A.L., V.G., A.B., V.T.; validation: A.L., V.G., V.T.; writing—original draft: V.G.

Conflicts of Interest: The authors declare no conflict of interest. The sponsors had no role in the design, execution, interpretation, or writing of the study

References

1. Perkins, J.; Edwards, G.R.; Such, C.R.; Johnson, J.M.; Alten, R.R. Thermomechanical characteristics of alloys exhibiting martensitic thermoelasticity. In *Shape Memory Effects in Alloys*, 1st ed.; Perkins, J., Ed.; Plenum Press: New York, NY, USA, 1975; pp. 273–303.

2. Otsuka, K.; Shimizu, K.; Suzuki, Y.; Sekiguchi, Y.; Tadaki, K.; Honma, T.; Miyazaki, S. *Shape Memory Alloys*; Funakubo, H., Ed.; Gordon and Breach Science: New York, NY, USA, 1987; pp. 41–73.

3. Atli, K.C.; Karaman, I.; Noebe, R.D.; Garg, A.; Chumlyakov, Y.I.; Kireeva, I.V. Shape memory characteristics of $Ti_{49.5}Ni_{25}Pd_{25}Sc_{0.5}$ high-temperature shape memory alloys after severe plastic deformation. *Acta Mater.* **2011**, *59*, 4747–4760. [CrossRef]

4. Kockar, B.; Karaman, I.; Kim, J.I.; Chumlyakov, Y.I.; Sharp, J.; Yu, C.-J. (Mike) Thermomechanical cyclic response of an ultrafine-grained NiTi shape memory alloy. *Acta Mater.* **2008**, *56*, 3630–3646. [CrossRef]

5. Otsuka, K.; Ren, X. Physical metallurgy of Ti-Ni-based shape memory alloy. *Prog. Mater. Sci.* **2005**, *50*, 511–678.

6. Titanium Nickelide Alloys with Shape Memory. *Part 1. Structure, Phase Transitions, and Properties*; Pushin, V.G., Ed.; UB RAS: Ekaterinburg, Russia, 2006; pp. 72–169.

7. Brailovski, V.; Prokoshkin, S.; Terriault, P.; Trochu, F. *Shape Memory Alloys: Fundamentals, Modeling and Applications*; ETS Publ.: Montreal, QC, Canada, 2003; pp. 158–601.

8. Valiev, R.Z.; Aleksandrov, I.V. *Bulk Nonstructural Metal Materials: Production, Structure and Properties*; Akademkniga: Moscow, Russia, 2007; pp. 55–349.

9. Gunderov, D.; Lukyanov, A.; Prokofiev, E.; Kilmametov, A.; Pushin, V.; Valiev, R.Z. Mechanical properties and martensitic transformations in nanocrystalline Ti49.4Ni50.6 alloy produced by high-pressure torsion. *Mater. Sci. Eng. A* **2009**, *503*, 75–77. [CrossRef]

10. Lotkov, A.I.; Grishkov, V.N.; Dudarev, E.F.; Girsova, N.V.; Tabachenko, A.N. The formation of ultrafine-grained state, martensitic transformations and inelastic properties of titanium nickelide after "abc"-pressing. *Vopr. Mater.* **2008**, *1*, 161–165.

11. Nakayama, K.; Tsuchiya, K.; Umemoto, M. Crystal refinement and amorphization by cold rolling. *JMNM* **2003**, *15–16*, 283–288. [CrossRef]

12. Mohamed, H.A.; Washburn, J. Deformation behaviour and shape memory effect of near-equiatomic NiTi alloy. *J. Mater. Sci.* **1977**, *12*, 469–480. [CrossRef]

13. Hornbogen, E. Ausforming of NiTi. *J. Mater. Sci.* **1999**, *34*, 599–606. [CrossRef]

14. Sehitoglu, H.; Jun, J.; Zhang, X.; Karaman, I. Shape memory and pseudoelastic behavior of 51.5%Ni–Ti single crystals in solutionized and overaged state. *Acta Mater.* **2001**, *49*, 3609–3620. [CrossRef]

15. Prokoshkin, S.D.; Brailovski, V.; Inaekyan, K.E.; Demerus, V.; Khmelevskaya, I.Yu.; Dobatkin, S.V.; Tatyanin, E.V. Structure and Properties of Severely Cold-Rolled and Annealed Ti-Ni Shape Memory Alloys. *Mater. Sci. Eng. A* **2008**, *481–482*, 114–118. [CrossRef]

16. Karaman, I.; Karaca, H.E.; Luo, Z.P.; Maier, H.J. The effect of severe marforming on shape memory characteristics of a Ti-rich NiTi alloy processed using equal channel angular extrusion. *Metall. Mater. Trans. A* **2003**, *34*, 2527–2539. [CrossRef]

17. Gunderov, D.V.; Prokofiev, E.A; Pushin, V.G.; Valiev, R.Z. On the nature of high strength and plasticity in ultrafine-grained TiNi produced by equal channel angular pressing. Deform. *Razrush. Mater.* **2007**, *10*, 13–21.

18. Pushin, V.G.; Lotkov, A.I.; Kolobov, Yu.R.; Valiev, R.Z.; Dudarev, E.F.; Kuranova, N.N.; Dyupin, A.P.; Gunderov, D.V.; Bakach, G.P. On the Nature of Anomalously High Plasticity of High-Strength Titanium Nickelide Alloys with Shape-Memory Effects: I. Initial Structure and Mechanical Properties. *Phys. Met. Metallogr.* **2008**, *106*, 520–530. [CrossRef]

19. Pops, H. Stress-Induced Pseudoelasticity in Ternary Cu-Zn Based Beta Prime Phase Alloys. *Met. Trans.* **1970**, *1*, 251–258.

20. Warlimont, H.; Delay, L. *Martensitic Transformation in Cooper-, Silver- and Gold-Based Alloys*; Pergamon: Oxford, UK, 1974; pp. 113–135.

21. Wayman, C.M.; Duerig, T.W. An Introduction to Martensite and Shape Memory. In *Engineering Aspects of Shape Memory Alloys*, 1st ed.; Wayman, C.M., Duerig, T.W., Eds.; Butterworth-Heineman: London, UK, 1990; pp. 3–20.

22. Cross, W.B.; Kariotis, A.H.; Stimler, F.J. *Nitinol Characterization Study*; NASA: Langley, VA, USA, 1969, CR-1433; pp. 1–60.

23. Wasilewski, R.J. The shape memory effect in TiNi: one aspect of stress-assisted martensitic transformation. In *Shape Memory Effects in Alloys*, 1st ed.; Perkins, J., Ed.; Plenum Press: New York, NY, USA, 1975; pp. 245–270.

24. Melton, K.N.; Mercier, O. Deformation Behavior of NiTi-Based Alloys. *Met. Trans. A* **1970**, *9A*, 1487–1488. [CrossRef]

25. Miyazaki, S.; Otsuka, K.; Suzuki, Y. Transformation pseudoelasticity and deformation behavior in Ti-50.6at%Ni alloy. *Scripta Metall.* **1981**, *15*, 287–292. [CrossRef]

26. Piao, M.; Otsuka, K.; Miyazaki, S.; Horikawa, H. Mechanism of the A_S temperature increase by pre-deformation in thermoelastic alloys. *Mater. Trans.* **1993**, *34*, 919–929. [CrossRef]

27. Roumagnac, P.; Guillemer-Neel, C.; Saanouni, K.; Clavel, M. Mechanical behavior and deformation mechanisms of Ni-Ti shape memory alloys in tension. *Eur. Phys. J.* **2000**, *AP10*, 109–122.

28. Lu, Y.; Xie, Z.; Humbeeck, J.V.; Delay, L.; Liu, Y. On the deformation of the twined domain in NiTi shape memory alloys. *Phil. Mag. A* **2000**, *80*, 1935–1953. [CrossRef]

29. Tan, G.; Liu, Y. Comparative study of deformation-induced martensite stabilization via martensitic reorientation transformation in NiTi. *Intermetallics* **2004**, *12*, 373–381. [CrossRef]

30. Zang, J.X.; Sato, M.; Ishida, A. Deformation mechanism of martensite in Ti-rich Ti-Ni shape memory alloy thin films. *Acta Mater.* **2006**, *54*, 1185–1198. [CrossRef]

31. Liu, Y.; Tan, G.; Miyazaki, S. Deformation-induced martensite stabilization in [100] single-crystalline Ni-Ti. *Mater. Sci. Eng. A* **2006**, *438–440*, 612–616. [CrossRef]

32. Surikova, N.S.; Evtushenko, O.V.; Pavlyuk, V.A. Strain localization and temperature dependence of yield stress in TiNi-based single crystals. *Phys. Mesomech.* **2010**, *1–2*, 96–102. [CrossRef]

33. Ezaz, T.; Wang, J.; Sehitoglu, H.; Maier, H.J. Plastic deformation of NiTi shape memory alloys. *Acta Mater.* **2012**, *61*, 67–78. [CrossRef]

34. Tadayyon, G.; Guo, Y.; Mazinani, M.; Zebarjad, S.M.; Tiernan, P.; Tofail, S.A.M.; Biggs, M.J.P. Effect of different stages of deformation on microstructure evolution of Ti-rich NiTi shape memory alloy. *Mater. Charact.* **2017**, *125*, 51–66. [CrossRef]

35. Lotkov, A.; Grishkov, V.; Timkin, V.; Baturin, A.; Zhapova, D. Yield stress in titanium nickelide-based alloys with thermoelastic martensitic transformations. *Mater. Sci. Eng. A* **2019**, *744*, 74–78. [CrossRef]

36. Lotkov, A.I.; Kashin, O.A.; Grishkov, V.N.; Krukovskii, K.V. The influence of degree of deformation under isothermal abc pressing on evolution of structure and temperatures of phase transformations of alloy based on titanium nickelide. *Inorg. Mater. Appl. Res.* **2015**, *6*, 96–104. [CrossRef]

37. Prokoshkin, S.; Dubinskiy, S.; Brailovski, V.; Korotitskiy, A.; Sheremetyev, S.; Blinova, E. Nanostructures and stress-induced phase transformation mechanism in titanium nickelide annealed after moderate cold deformation. *Mater. Lett.* **2017**, *192*, 111–114. [CrossRef]

38. Lotkov, A.; Grishkov, V.; Zhapova, D.; Timkin, V.; Baturin, A.; Kashin, O. Superelasticity and shape memory effect after warm abc-pressing of TiNi-based alloy. In Proceedings of the 2nd Conference on Shape Memory Alloys, SMA 2016, St Petersburg State University, St Petersburg, Russia, 20–23 September 2016; Belyaev, S., Prokoshkin, S., Razov, A., Volkov, A., Resnina, N., Eds.; Mater. Today Proc.: Amsterdam, The Netherlands, 2017. 4 (3PB). pp. 4814–4818.